Microstructure of Thin-Wall Ductile Iron Castings

Ö.N. Doğan, K.K. Schrems, J.A. Hawk,
U.S. Department of Energy, Albany Research Center, Albany, Oregon 97321

ABSTRACT

Step plate castings with section thicknesses of 1.5 mm to 6 mm and individual (single) castings with section thicknesses of 2 mm to 6 mm were produced using a ductile iron chemistry. Microstructures of these thin wall ductile iron castings were characterized quantitatively using an image analyzer. Matrix structure and (amount of pearlite, ferrite, and massive carbides), graphite structure (volume fraction, nodule size, nodule count, and nodularity) were investigated as a function of section thickness. Pearlite content, nodule count, and nodularity increased with decreasing section thickness, whereas the nodule size decreased. Nodule count exceeded 2000 nodules per mm^2 at the thinnest sections. Statistical analysis was performed to investigate the effect of casting parameters on the microstructure.

INTRODUCTION

The US transportation industry is faced with three major challenges: reduce emissions, improve fuel economy, and lower cost. One method of improving fuel economy is to reduce vehicle weight (a vehicle weight reduction of 250 pounds (113.6 kg) is commonly equated to a fuel economy improvement of 1 mpg). In the 1970's, the automotive industry reduced vehicle weight by reducing the thickness of steel sheet (driving the development of high-strength low-alloy steels and corrosion resistant coatings). In the 1980's and the early 1990's, vehicle weight was further reduced by substituting aluminum for cast iron and steel (primarily in cylinder heads, engine blocks and wheels). Currently, the substitution of aluminum for cast iron and steel, and magnesium for aluminum is continuing. The use of aluminum, however, results in higher vehicle costs, which are passed on to the consumer. To provide the transportation industry with a means of weight reduction at little or no cost penalty, the cast iron and steel industries have undertaken major product improvement programs, e.g., thin-wall iron casting technology and lightweight steel body technology. Recent research (Javaid, 1999; Javaid, 2000; Labrecque, 2000) has shown the feasibility of producing thin-wall iron castings. Commercially viable, lightweight cast iron technology is being developed by TWIG (Thin-Wall Iron Group) through a cooperative program with major US foundry companies, foundry suppliers, the Big 3 automakers, the University of Alabama, and U.S. Department of Energy Albany Research Center. TWIG has launched programs specifically focused on control of microstructure, solidification modeling, and dimensional capability in thin section castings, generation of useful mechanical property data.

The current paper presents the results of microstructural characterization of thin wall ductile iron castings. Mechanical properties obtained from the same castings are presented elsewhere (Schrems, 2003).

EXPERIMENTAL PROCEDURE

Melting and Casting: Three heats of nodular iron were produced using the open ladle treatment method for this study. Charges consisting of 200 lbs of nodular iron returns, 50 lbs (22.7 kg) of steel, 150 lbs (68.2 kg) of pig iron, 4.8 lbs (2.2 kg) of 75% foundry grade ferrosilicon and 2.4 lbs (1.1 kg) of carbon raiser were melted in a 500 lb (227.3 kg) coreless induction furnace.

Prior to treatment, the carbon content of the base irons were determined by thermal analysis using an Electro-Nite Quik-Cup QK-200, a Leeds & Northrup strip chart recorder and a BCIRA carbon calculator. The base irons had carbon contents of 3.80-3.95 wt% and silicon contents of 2.00-2.20 wt%. The irons were treated in a preheated transfer ladle containing 1.8 lbs (0.8 kg) of 3.5% magnesium-ferrosilicon, 1.1 lbs (0.5 kg) of 6% magnesium-ferrosilicon (Minoc) and 1.2 lbs (0.55 kg) of 75% foundry grade ferrosilicon. The manufacturer's analyses of these ferrosilicon alloys are listed in Table 1. Treatment temperature was 2770°F-2780°F (1521°C-1527°C).

Upon completion of treatment, reaction products that floated to the melt surface were skimmed. At this time, samples for chemical analysis were taken. The chemistries of the samples were determined using a Baird DV-6 spectrometer. Carbon

was not analyzed for after treatment but was calculated knowing that it would be 0.13 wt% less than the base iron carbon content. The final chemistries of the three heats are listed in Table 2.

The treated irons were poured into dry sand molds bonded with pepset resin. The irons were post-inoculated using two methods: for heat 6, 75% foundry grade ferrosilicon was placed in the mold and for heats 8 & 9, 75% foundry grade ferrosilicon was added to the stream during pouring. For all heats, eight molds were poured. The pouring temperature ranges for the first and last molds were 2670°F -2680°F (1466°C-1471°C) and 2620°F -2630°F (1438°C-1443°C), respectively. The manufacturers analysis of the in-stream ferrosilicon is listed in Table 1.

The test castings were thin strips approximately 25 mm wide by 100 mm long with a 25 mm x 25 mm x 35 mm runoff and a step plate consisting of joined strips approximately 25 mm wide by 100 mm long. The thicknesses of the strips were 1.5, 2.0, 2.5, 3.0, 3.5, 4.0, 5.0 and 6.0 mm. The test casting is shown in Figure 1. Pour time for these castings was approximately 5 seconds. Shake-out time was approximately 120 minutes. The castings were cleaned with a wire brush to prevent distortion.

Table 1. Manufacturer's Analyses of Treatment Alloy, Ferrosilicon and Post Inoculants.

Element	3.5% Mg-FeSi	Minoc	75% FeSi	In-Stream 75% FeSi
Mg	3.52	6.30		
Si	45.02	45.40	75.0	75.0
TRE*	0.49	0.62		
Al	0.72	0.65	1.05	
Ca	0.59	0.49	0.65	
Fe	balance	balance	balance	balance
sizing	5/8" x 18 mesh	18 x 100 mesh	5 x 18 mesh	30 x 80 mesh

* total rare earths

Table 2. Final Composition of Treated Irons.

Element	Heat TW-6	Heat TW-8	Heat TW-9
C	3.87	3.85	3.89
Si	2.74	2.67	2.67
Mn	0.22	0.20	0.21
Cu	0.15	0.10	0.14
Cr	0.05	0.04	0.04
Mg	0.020	0.021	0.021
S	0.006	0.006	0.009

Microstructural Analysis: Microstructural specimens were taken from the center of each single casting and each step of the step plate castings. The specimens were mounted, ground, and polished using the conventional metallographic techniques.

Image analysis was performed using an Optimas 6.2 image analysis software. Images acquired were 640 x 480 pixels with a resolution of 204 pixels per inch. Images were acquired at a magnification of 224x. Thus, one pixel represented a linear distance of 0.59 µm on the images. Polished but unetched samples were used to measure features of graphite nodules. Ten fields of view per sample were analyzed. The basic features measured were number, Feret diameters, area fraction, area, and

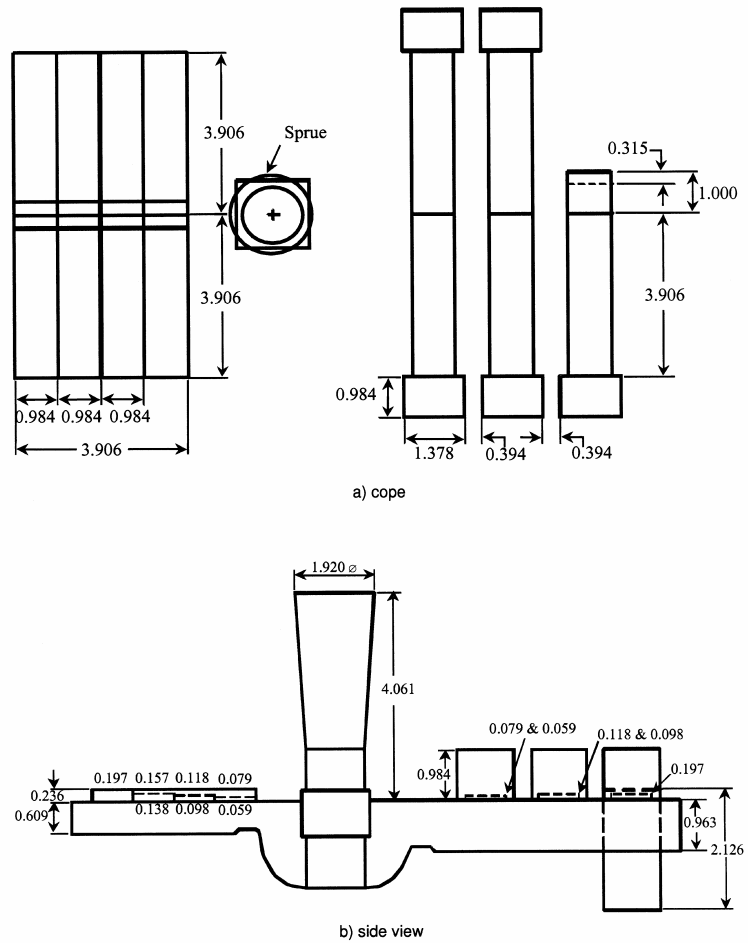

Figure 1 Foundry pattern used to create step plate castings (left) and single castings (right). Measurements in mm.

perimeter of two dimensional sections of graphite particles on the plane of polish. When measuring the basic features, "minimum boundary length" of a particle was set to 5 µm. This is equivalent to a circle with a diameter of 1.59 µm. Particles smaller than this were not measured. From these basic measurements, other properties such as sphericity and compactness were calculated. Furthermore, various nodularity values were calculated from sphericity and compactness values. When calculating the derived properties, only the particles with a diameter greater than 10 pixel size were considered. In a few samples, this meant that only those particles larger than the average diameter were taken into account in nodularity calculations.

Nodularity of graphite particles was calculated using both area and number of acceptable and unacceptable particles as shown below.

$$\%\,Nodularity = \frac{area\ (number)\ of\ acceptable\ particles}{area\ (number)\ of\ all\ particles} \qquad \text{Equation 1}$$

The criterion for an acceptable particle was compactness ≥ 0.70 or sphericity ≥ 0.65. Compactness and sphericity for each nodule are defined as follows:

$$Compactness = 4\pi \frac{Area}{ConvexPerimeter^2} \qquad \text{Equation 2}$$

$$Sphericity = 4\pi \frac{Area}{Perimeter^2}$$ Equation 3

Matrix of the castings was characterized after etching the samples with 4% Nital. Amount of pearlite (area fraction of pearlite on the plane of polish) was calculated by subtracting the graphite content (area fraction of graphite on the plane of polish) from the fraction of dark regions in the field of view on the plane of polish. The samples were etched with Klemm's reagent and $Na_2S_2O_5$ + picric acid solution to reveal carbides.

Statistical Analysis of Microstructural Features: A total of eight dependent variables were fit to combinations of explanatory (independent) variables. The explanatory variables consisted of indicator variables for the casting heat (TW8 was chosen as the baseline) and single/step plate configuration, and a continuous variable for thickness effects. Indicator variables have a value of one if the variable is true, e.g., *single* = 1for a single casting, and a value of zero if the variable is false, e.g., *single* = 0 for a step plate casting. Five different variables were examined for thickness: t_u, $1/t_u$, $(1/t_u)^2$, SA/v, and $(SA/v)^2$, where t_u is the unground thickness, SA is the effective surface area, and v is the volume. The eight dependent variables were the count of nodules per mm^2, compactness, sphericity, nodularity % (count, compactness), nodularity % (area, compactness), nodularity % (count, sphericity), nodularity % (area, sphericity), and pearlite %. For each thickness variable, a full model consisting of the thickness variable, single/step plate indicator, and casting heat indicator was run. After recording the adjusted R^2 and model p-value, forwards and backwards stepwise multiple linear regression procedures were run to eliminate parameters that did not contribute significantly to the model. The forward stepwise regression procedure had a generous f-to-enter of 1 and f-to-remove of 0. The backwards stepwise regression procedure had a more stringent f-to-enter of 11 and f-to-remove of 10.

RESULTS AND DISCUSSION

Three heats of castings were produced using the same procedure except for the post inoculation method. Post inoculation in the runner was used for the castings of heat TW-6 and stream post inoculation was used for the castings of heat TW-8 and TW-9. This was the only deliberate difference among these heats.

Most models had p-values < 0.00001, which indicates that the models are highly significant. There is little chance that the data occurred by chance. Secondly, using the unground thickness was also found to be significant, but the explanatory power of the models was considerably less than the other thickness measurements used. The parameter $(1/t_u)^2$ often produced the best fit model, followed by $(1/t_u)$, but the explanatory power of the $1/t_u$ and (SA/V) and the squared models often differed by less than 2%. Surprisingly, the SA/V models were designed to account for the differences in cooling rate between singles and step plates, but often resulted in the single indicator variable remaining in the model. The SA/V models do not appear to account for the differences between singles and step plates. The choice of variable to use for thickness should reflect the physical situation. The parameters $1/t_u$ and SA/v can be directly attributed to a cooling rate effect while the parameters $(1/t_u)^2$ and $(SA/V)^2$ are inversely proportional to solidification time through Chvorinov's rule (Flemings, 1974).

PEARLITE CONTENT

Pearlite content of microstructure varies with thickness of castings. In general, the pearlite content decreases with increasing thickness of castings (Figure 2). An increase in the pearlite content at the thickest sections was observed in the step plate castings.

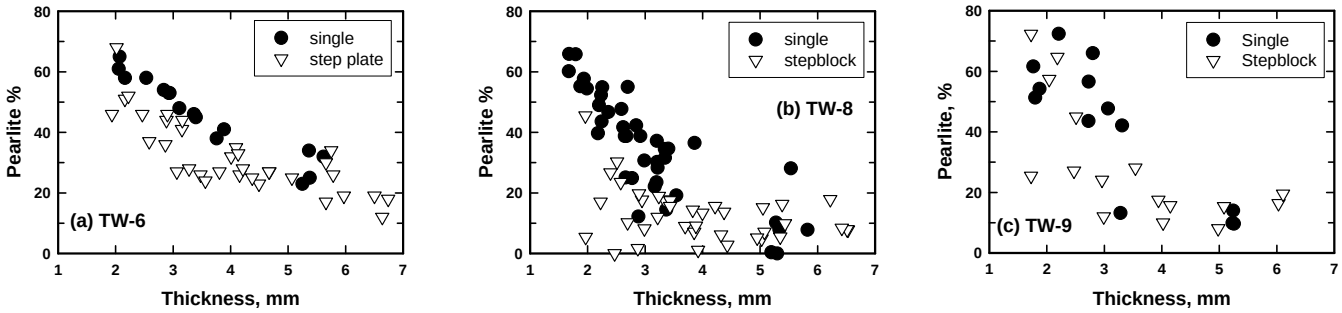

Figure 2 Pearlite content of thin wall castings as a function of section thickness. (a) TW-6, (b) TW-8, and (c) TW-9.

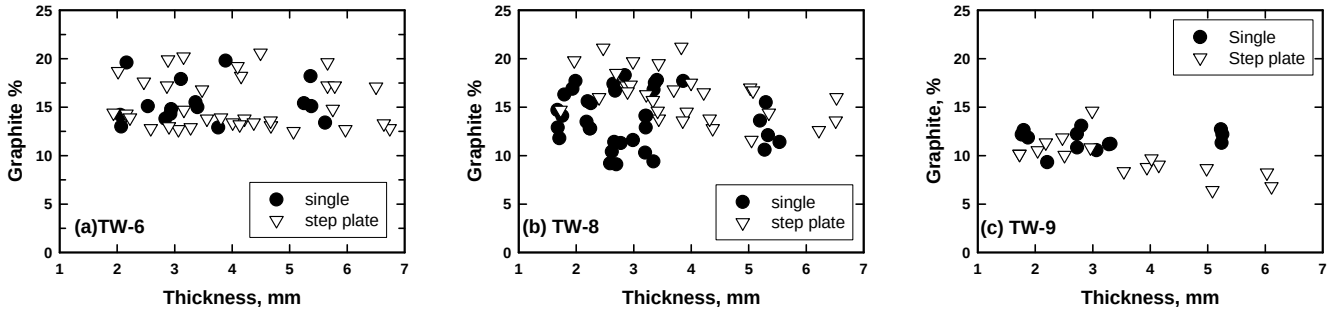

Figure 3 Volume fraction of graphite in the thin wall castings. (a) TW-6, (b) TW-8, and (c) TW-9.

In the TW-6 castings, the pearlite content varies from above 60% in the thinnest sections to below 20% in the thickest sections as shown in Figure 2a. Generally, the step plate samples contain less pearlite than the single samples for a given thickness.

In the single specimens of the TW-8 castings, the pearlite content increases as the thickness decreases as shown in Figure 2b. The thinnest castings (~2 mm) contain about 50-65% pearlite whereas the thickest sections (~6 mm) contain about 0-10% pearlite. Pearlite content of step plates do not show similar dependency on thickness in the TW-8 castings. The pearlite content is generally lower in the step plates. Even in the thinnest sections, it is well below 50%. The thicker sections have a pearlite content of 0-20%.

Pearlite content of the step plate samples in the TW-9 castings were also lower than that of the single castings for a given section thickness at the thin sections (Figure 2c). At the thicker sections, they had similar amount of pearlite.

The regression model for the amount of pearlite was found to be highly significant ($p<0.0001$) and had an adjusted R^2 of approximately 0.73. The parameter ($1/t_u$) was found to produce the best fit with the data. This reflects the strong dependence of pearlite on the cooling rate. TW6, TW9, and single were found to be significant and remained in the model through the forward and backwards stepwise procedure for all measures of thickness. The amount of pearlite is different between the three casting heats as well as between the singles and the step plates. Chemistry, pouring temperature, and time between inoculation and solidification probably account for some of the differences. A good model for the mean value of pearlite (%) can be expressed as:

$$pearlite(\%) = \underset{(2.6)}{-16.2} + \underset{(7.0)}{106.7}/t_u + \underset{(1.6)}{12.4}*\text{single} + \underset{(1.9)}{18.1}*\text{TW6} + \underset{(2.0)}{9.5}*\text{TW9} \qquad \text{Equation 4}$$

where the standard error of the coefficients is presented below the model.

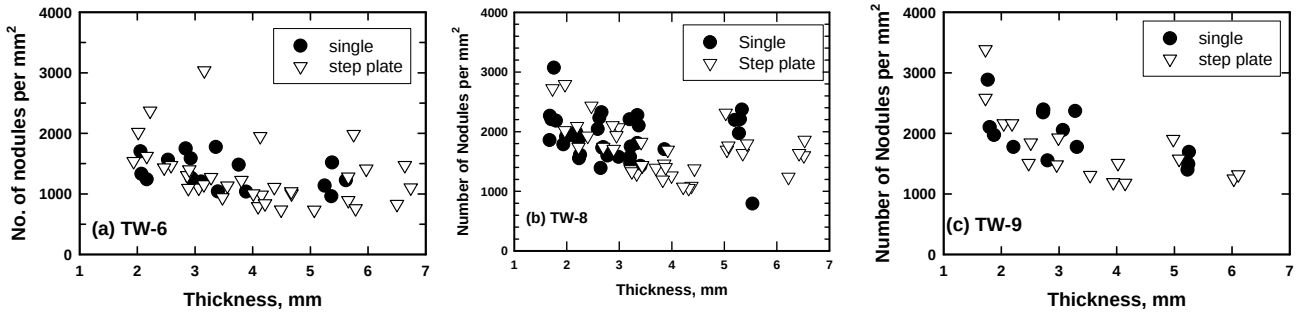

Figure 4 Nodule count in the thin wall ductile iron castings. (a) TW-6, (b) TW-8, (c) TW-9.

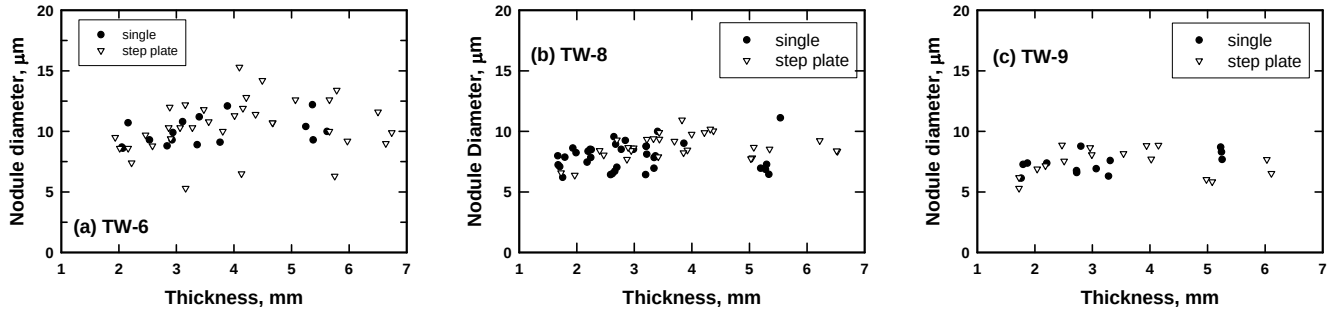

Figure 5 Nodule size in the thin wall ductile iron castings. (a) TW-6, (b) TW-8, and (c) TW-9.

CARBIDE CONTENT

No massive carbides were revealed on the metallographic samples of castings of TW-6, TW-8, and TW-9 using two different etchants.

GRAPHITE CONTENT

Graphite content in the TW-6, TW-8, and TW-9 castings varied dramatically from sample to sample. However, the graphite content of the single castings did not change significantly with casting thickness in all three groups of castings as shown in Figure 3. Amount of the graphite phase varies between 13 to 20 % in the TW-6 single castings, 9-18 % in the TW-8 single castings, and 9-13 % in the TW-9 single castings regardless of casting thickness.

The graphite content in the step plates varies from about 7 to 22%. The graphite content of the step plates tends to decrease with increasing casting thickness.

NODULE COUNT

Number of graphite nodules decreased with increasing section thickness, in general, as shown in Figure 4. The nodule count decreased from about 1500 nodules per mm^2 at the 2 mm thick sections to about 1100 nodules per mm^2 at the 5.5 mm thick sections in the TW-6 single castings. In the TW-6 step plates, the nodule count decreased with increasing section thickness up to 4.5 mm and then it increased in the thickest sections as shown in Figure 4a. The nodule count was generally higher in TW-8 and TW-9 single castings (Figures 4b and 4c). The number of nodules varied, on average, from 2100 nodules per mm^2 in the TW-8 single castings and 2200 nodules per mm^2 in the TW-9 single castings at the 1.5 mm thick sections to 1900 and 1600 nodules per mm^2, respectively, at the 5.5 mm thick sections. The nodule count in the step plates of the TW-8 and TW-9 also decreased with increasing thickness up to 4.5 mm and then it increased in the thickest sections. The increase in the thickest sections of the step plates is because of the faster cooling due to the end effect.

The regression model for nodules/mm^2 was found to be highly significant ($p<0.0001$) with an adjusted R^2 of approximately 0.46. The parameter $(1/t_u)^2$ results in the best fit. The indicator variable for TW9 drops out of the model, which reflects the similarity in inoculation practices between TW8 and TW9. TW6 was post-inoculated in the mold while TW8 and TW9 were inoculated in the stream. In this investigation, the stream inoculation was more effective in providing nucleation sites for the eutectic cells of the ductile iron. Although the indicator variable for single/step plate status was not significant, it did add some explanatory power to the model. It was usually eliminated by the backwards stepwise procedure. A good model for nodules/mm^2 can be expressed as:

$$nodules/mm^2 = \underset{(55.4)}{1394} + \underset{(327)}{3000/t_u^{\,2}} - \underset{(64.3)}{365}*(TW6) \qquad \text{Equation 5}$$

where the standard error of the coefficients is presented below the model. All parameters were found to be significant.

GRAPHITE NODULE SIZE

As shown in Figure 5, average graphite nodule diameter is generally higher in the castings of heat TW-6 compared to the castings of heats TW-8 and TW-9. For example, in the single castings, average nodule diameter is about 10 µm for the TW-6 castings while it is 8 µm for the TW-8 castings, and 7 µm for the TW-9 castings. In addition, the nodule size increases slightly with increasing section thickness in the single castings.

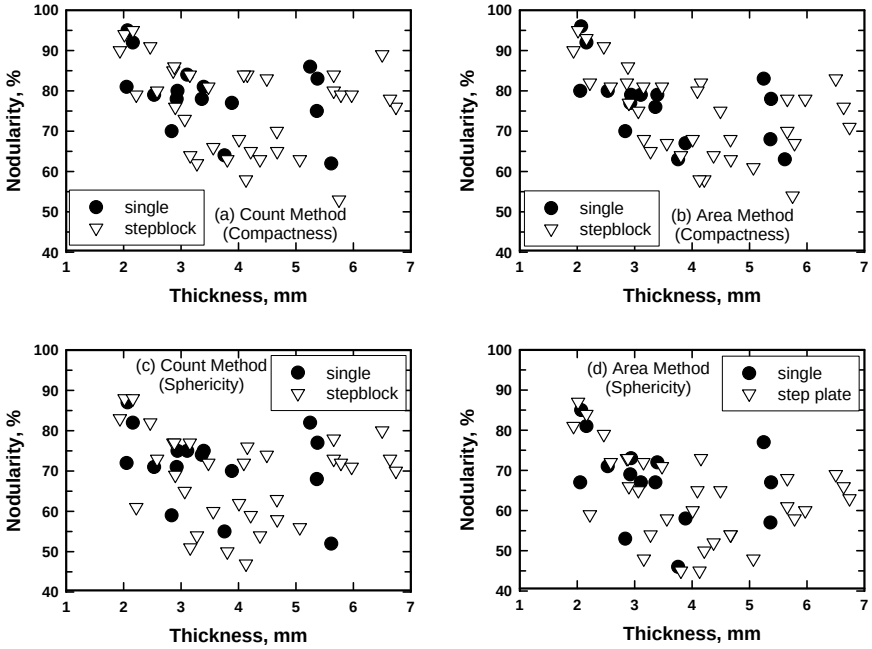

Figure 6 Nodularity of graphite phase in TW-6 thin wall ductile iron samples as determined by different methods. (a) Count method using compactness as acceptability criterion, (b) Area method using compactness as acceptability criterion, (c) Count method using sphericity as acceptability criterion, (d) Area method using sphericity as acceptability criterion.

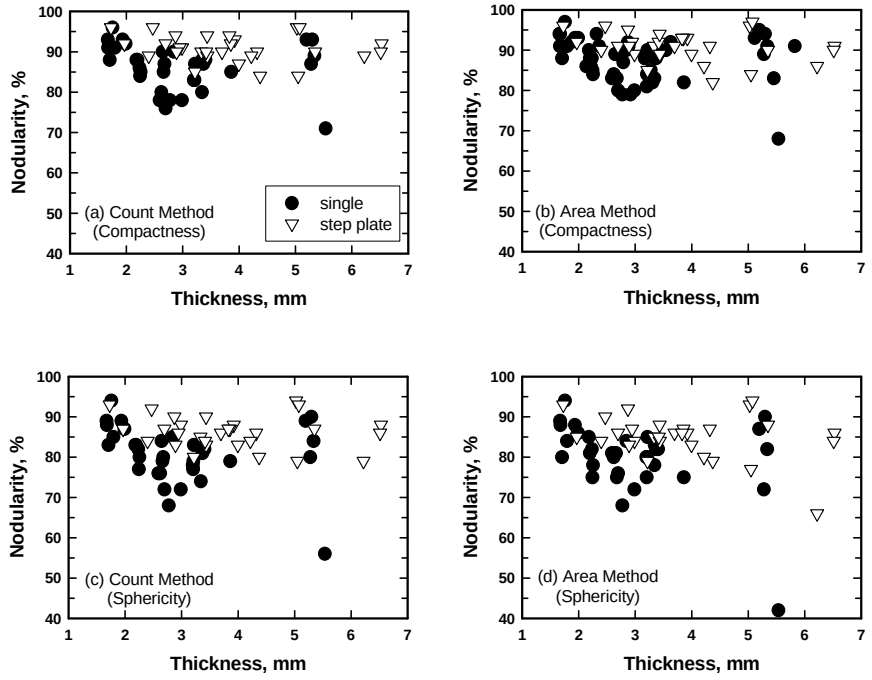

Figure 7 Nodularity of graphite phase in TW-8 thin wall ductile iron samples as determined by different methods. (a) Count method using compactness as acceptability criterion, (b) Area method using compactness as acceptability criterion, (c) Count method using sphericity as acceptability criterion, (d) Area method using sphericity as acceptability criterion.

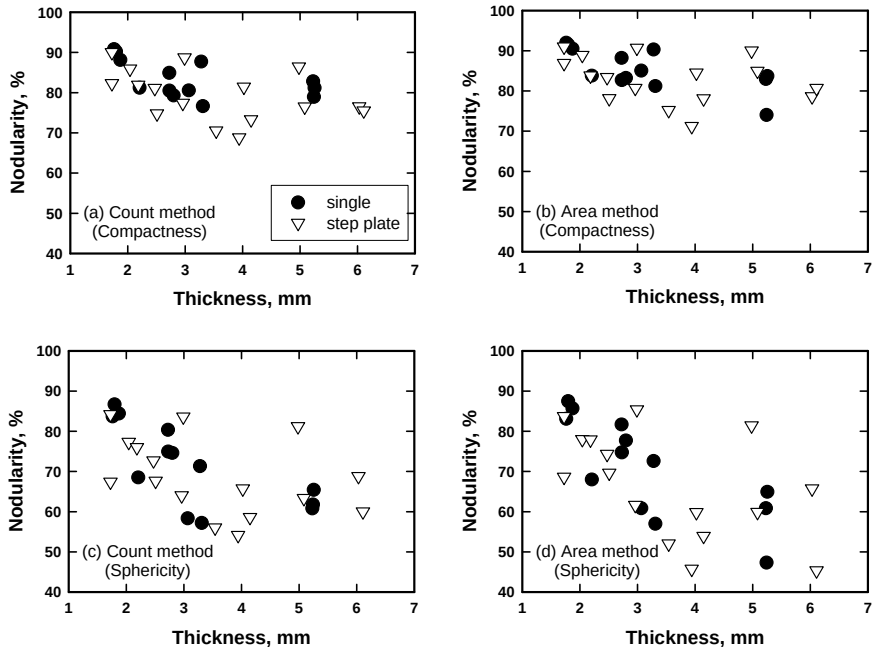

Figure 8 Nodularity of graphite phase in TW-9 thin wall ductile iron samples as determined by different methods. (a) Count method using compactness as acceptability criterion, (b) Area method using compactness as acceptability criterion, (c) Count method using sphericity as acceptability criterion, (d) Area method using sphericity as acceptability criterion.

The increase in the graphite nodule size in the step plates with increasing thickness is faster than the single castings up to 4.5 mm thick sections. At the thickest sections of the step plates, the graphite nodule size decreases as the cooling rate increases due to the end effect.

NODULARITY

Figures 6 through 8 show the nodularity of graphite in each casting of heats TW-6, TW-8, and TW-9 as determined using different methods. In general, the nodularity of castings was lower when sphericity of particles was the acceptance criterion when either the count or the area method was used.

Nodularity in TW-6 castings decreased with increasing section thickness in both the single castings and step plates up to a section thickness of approximately 4 mm (Figure 6). For the thicker sections, the nodularity increased again (to above 70% in the case of area method with compactness used as the acceptance criterion as shown in Figure 6a). For a given section thickness, the nodularity was similar for both the single and step plate castings. The nodularity in the TW-6 castings ranged from above 90% in the thinnest sections to 60% in some of the thicker castings.

The TW-8 castings had generally higher nodularity as shown in Figure 7. Nodularity of most castings in this heat was above 80% when the compactness was used as the acceptance criterion, and above 70% when the sphericity was the acceptance criterion. Even in the thicker sections, the average nodularity was high in the TW-8 castings. Although the nodularity did not change significantly with section thickness, the thinnest sections of TW-8 contained nodules with a slightly higher nodularity.

The nodularity of the TW-9 castings decreased with decreasing cooling rate (Figure 8). The nodularity varied from about 92% in the thinnest sections to the 72% in the 4 mm step plate section. For the thicker sections of the step plates, the nodularity went back up again except for one 6 mm section which retained a low nodularity.

The lower nodularity values for the TW-6 castings compared to the TW-8 and TW-9 castings are thought to be a result of the inoculation method. The TW-6 castings were inoculated in mold as opposed to the stream inoculation of the TW-8 and TW-9 castings. The stream inoculation in this investigation was more effective in providing nucleation sites for the eutectic cells. As a result, the TW-8 and TW-9 castings had a higher nodule count and finer graphite nodules promoting higher nodularity.

Compactness was found to have the best model when $(1/t_u)^2$ was used. The indicator variable for single always dropped out and the indicator variables for TW6 and TW9 always remained. The model accounted for 37.9% of the variation in the data. This model can be expressed as:

$$\underset{}{compactness} = \underset{(0.006)}{0.831} + \underset{(0.03)}{0.157}/t_u^{\,2} - \underset{(0.007)}{0.466} * TW6 - \underset{(0.006)}{0.460} * TW9 \qquad \text{Equation 6}$$

This is in contrast to the model for sphericity, which accounted for 44.5% of the variation in the data. The parameter $(1/t_u)^2$ or $(ESA/v)^2$ produced the best fit. The indicator variable for single would usually drop out, but it remained through the forward stepwise procedure for the ESA/v terms. TW6 and TW9 always remained in the model. This model can be expressed as:

$$\underset{}{sphericity} = \underset{(0.007)}{0.744} + \underset{(0.04)}{0.203}/t_u^{\,2} - \underset{(0.008)}{0.064} * TW6 - \underset{(0.007)}{0.062} * TW9 \qquad \text{Equation 7}$$

Given a choice between compactness and sphericity, the data fits a model for sphericity better than compactness. At this point, it is unknown whether the model for sphericity is a better fit or whether the data for compactness has more variation. This could be investigated further. Note also the coefficients for TW6 and TW9. For both compactness and sphericity, the coefficients are similar in direction and magnitude. In setting up this model, it was assumed that TW8 and TW9 would behave similarly and that TW9 would drop out of the model. This does not occur. TW6 and TW9 behave similarly to each other in a manner different from that of TW8. This is unexpected.

The explanatory difference between the models based on compactness and sphericity are reflected in the remaining dependent variables. Nodularity % count (compactness) had an adjusted R^2 of 0.372 compared to the value for nodularity % count (sphericity) of 0.450. Again, the parameters $(1/t_u)^2$ or $(SA/v)^2$ usually produced the best fit, TW6 and TW9 remained in the model, and single usually dropped out, although later for the SA/v terms. These models can be expressed as:

$$\underset{}{nodularity\ \%\ (count, compactness)} = \underset{(1.2)}{84.2} + \underset{(6.2)}{31.4}/t_u^{\,2} - \underset{(1.3)}{10.3} * TW6 - \underset{(1.3)}{7.5} * TW9 \qquad \text{Equation 8}$$

$$\underset{}{nodularity\ \%\ (count, sphericity)} = \underset{(1.4)}{77.9} + \underset{(7.2)}{41.0}/t_u^{\,2} - \underset{(1.6)}{12.9} * TW6 - \underset{(1.5)}{13.4} * TW9 \qquad \text{Equation 9}$$

Nodularity % (area, compactness) had an adjusted R^2 of 0.473 versus a value of 0.504 for nodularity % (area, sphericity). Again, TW6 and TW9 remained in the models. The indicator variable for single/step plate would generally drop out during the backwards stepwise regression procedure. Of more interest is that $(1/t_u)^2$ or $(SA/v)^2$ produced the best models for nodularity % (area, compactness) and $(1/t_u)$ or (SA/v) produced the best models for nodularity % (area, sphericity). However, the differences between the explanatory power of the models is about 0.5%, so this may be random. Since $(1/t_u)^2$ is proportional to the solidification time, these models can be expressed as:

$$\underset{}{nodularity\ \%\ (area, compactness)} = \underset{(1.1)}{84.4} + \underset{(5.9)}{34.6}/t_u^{\,2} - \underset{(1.3)}{12.7} * TW6 - \underset{(1.3)}{5.1} * TW9 \qquad \text{Equation 10}$$

$$\underset{}{nodularity\ \%\ (area, sphericity)} = \underset{(1.6)}{75.2} + \underset{(8.2)}{56.0}/t_u^{\,2} - \underset{(1.8)}{17.2} * TW6 - \underset{(1.8)}{13.6} * TW9 \qquad \text{Equation 11}$$

FADE OF INOCULANTS:

It can be generally said that the previous models account for the effects of cooling rate by the use of single/step plate indicator variable and the unground thickness as well as chemical composition by the use of indicator variables for the casting heats. It is well known that inoculants and nodulizers depend on time, i.e., their effect 'fades' with time. Although there is no time-based variable available for TW8 and TW9, an approximation can be made with TW6. TW6 was received as a series of complete castings that were cast from a single chemical composition. Castings marked 2, 3, 4, 5, and 7 were

received. During sample preparation, these casting numbers were maintained. As such, a reduced spreadsheet containing only TW6 was evaluated. Indicator variables were included to identify castings 3, 4, 5, and 7, although it is not known if these are sequential. Although these designations are used to approximate a time-based effect on inoculation and nodularization, this effect will be confounded with pouring temperature. Nonetheless, the results have been enlightening.

The full model took the form:

$$dependent\ variable = \beta_0 + \beta_1 / t_u^{\,2} + \sum \left\{ \beta_i * (casting\ i) \right\} \qquad \text{Equation 12}$$

where i = 3,4,5, and 7. A reduced model took the form:

$$dependent\ variable = \beta_0 + \beta_1 / t_u^{\,2} \qquad \text{Equation 13}$$

These results are presented in Table 3.

Several trends can be observed from this data. First, most models drop dramatically in explanatory power (adjusted R^2) in going from the full to the reduced model. This indicates that the casting number accounts for a significant amount of the variation in the data, and suggests that there is a time-based effect on the microstructural parameters. For example, nodularity %area (compactness) can be calculated as follows:

$$\begin{aligned} nodularity\ \%area\ (sphericity) = {} & 61.2 + 86.2 / t_u^{\,2} + 4.7 * \text{single} + 0.74 * (casting\ 3) - 7.8 * (casting\ 4) - 9.5 * (casting\ 5) - 26.1 * (casting\ 7) \\ & (2.3)\ (13.3) \qquad (2.0) \qquad (2.9) \qquad (2.5) \qquad (2.5) \qquad (2.9) \end{aligned}$$

Equation 14

The p-value for casting 3 is not significant. A single casting has a nodularity number 4.7 higher than a step plate. Specimens from casting 4 have a nodularity value 7.8 less than casting 2. Casting 7 has a nodularity value 26.1 less than casting 2.

Table 3. Results of models showing the effect of fading of inoculants

Dependent Variable	Full Model		Reduced Model	
	adjusted R^2	p-value	adjusted R^2	p-value
nodules/mm^2	0.593	0.000000	0.179	0.001157
compactness	0.678	0.000000	0.210	0.000431
sphericity	0.699	0.000000	0.181	0.001082
nodularity % count (compactness)	0.660	0.000000	0.254	0.000097
nodularity % area (compactness)	0.689	0.000000	0.447	0.000000
nodularity % count (sphericity)	0.681	0.000000	0.176	0.001277
nodularity % area (sphericity)	0.765	0.000000	0.343	0.000004
pearlite (%)	0.823	0.000000	0.698	0.000000
pearlite with $1/t_u^2$ and single			0.812	0.000000

Second, nodularity % area still shows a strong correlation with $1/t_u^2$ when the casting heat number is removed. It is unknown what the cause of this is.

Third, the amount of pearlite does not depend strongly on the casting number. Since the amount of pearlite is primarily related to cooling rate, this is not unexpected. Including the single/step plate indicator in the reduced model accounts for almost as much variation as when all the casting numbers are included.

Fourth, nodules/mm^2 doesn't show as good a correlation as the other variables. Since nodules/mm^2 depends on inoculation, and the inoculation was provided in-mold, this variable is not expected to show as strong an effect as the variables that depend on the effect of the nodulizer.

SUMMARY

Microstructure of ductile iron step plate castings with section thicknesses of 1.5 mm to 6 mm and individual (single) castings with section thicknesses of 2 mm to 6 mm were characterized quantitatively. The observations can be summarized as:

1. Pearlite content increases with decreasing thickness of castings.
2. Number of graphite nodules increases as the casting thickness decreases. It exceeds 2000 nodules per mm^2 in the thinnest sections.
3. Graphite nodules are generally finer in the thinnest sections.
4. Nodularity is generally above 80% in both the single and step plate castings.
5. All the sections examined were carbide free.

The exploratory data analysis showed that the models for image analysis data were all significant, although the explanatory power (adjusted R^2) tends to be low. This indicates that either there is significant scatter in the data or the models do not contain all the relevant explanatory variables. The analysis using the casting numbers for the TW6 castings suggests that a time-based variable to account for fade would reduce the scatter on most of the image analysis data. The amount of pearlite was not found to depend on the casting number.

ACKNOWLEDGMENTS

This research was conducted under ARC-DOE CRADA #0976 with the American Foundry Society in support of the DOE-OIT Project on Thin Wall Ductile Iron. The authors would like to acknowledge the financial support of AFS in supporting this cooperative research project between ARC, DOE Office of Industrial Technologies (Harvey Wong, Representative), AFS (Dr. Joe Santner, Project Coordinator), the University of Alabama (Dr. Tom Piwonka, University Coordinator), and the Thin Wall Iron Group consortium of companies (Dr. Alan Druschitz , Chair). Authors would like to acknowledge Kenneth Williamson of Albany Research Center for performing the image analysis. The authors also wish to express thanks to Intermet Corporation (Dr. Alan Druschitz) for providing the ductile iron samples used in this study.

REFERENCES

Flemings, M.C., *Solidification Processing,* p. 11*,* McGraw-Hill, Inc., New York, NY (1974)

Javaid, A., Thompson, J., Sahoo, M., Davis, K.G., "Factors Affecting the Formation of Carbides in Thin Wall DI Castings," *AFS Transactions*, vol 107, pp 441-456 (1999)

Javaid A., Davis, K.G., Sahoo, M., "Effect of Chemistry and Processing Variables on Mechanical Properties on Thin-Wall DI Castings," *AFS Transactions*, vol 108, pp 191-200 (2000)

Labrecque, C., Gagné, M., "Development of Carbide-Free Thin-Wall Ductile Iron Castings," *AFS Transactions*, vol 108, pp 31-38 (2000)

Schrems, K.K., Hawk, J.A., Doğan, Ö.N., Druschitz, A.P., "Statistical Analysis of the Mechanical Properties of Thin Walled Ductile Iron Castings," submitted to *SAE Transactions* (2003).